

Full Length Article

Gradient twinning microstructure generated by laser shock peening in an AZ31B magnesium alloy

Bo Mao^a, Yiliang Liao^{a,*}, Bin Li^b^a Department of Mechanical Engineering, University of Nevada, Reno, Reno, NV 89557, USA^b Department of Chemical and Materials Engineering, University of Nevada, Reno, Reno, NV 89557, USA

ARTICLE INFO

Keywords:

Mg alloys

Laser shock peening

Gradient microstructure

Deformation twinning

ABSTRACT

Mg alloys are lightweight structural metals that are promising for a variety of engineering applications. However, use of Mg alloys is often restricted by their poor mechanical properties. Recent studies indicate that a novel laser-based surface processing technology, laser shock peening (LSP), is promising to improve the engineering performance of Mg alloys by enhancing their surface strength, biocompatibility, fatigue resistance, and anti-corrosion ability. Despite these experimental efforts, little attention has been paid to study the surface microstructure evolution in the LSP process, particularly the formation of high density deformation twins. Deformation twinning in hexagonal closed-packed (HCP) crystal structure plays a fundamental role in enhancing mechanical performance of Mg alloys. This research is to establish the process-microstructure relationship of Mg alloys as processed by LSP. A focus is placed on understanding the deformation twinning mechanism. LSP experiments are conducted on a rolled AZ31B Mg alloy. The microstructures before and after laser processing are characterized. The effect of laser intensity on the twin volume fraction is investigated. The surface hardness as associated with the twin density is measured. The mechanism responsible for the formation of gradient twinning microstructure and the twinning-induced hardening effect are discussed. The anisotropic response to LSP in terms of grain orientation and the resultant microstructure and hardness improvement in the Mg samples are discussed.

1. Introduction

Mg alloys are lightweight structural metals that are promising for a variety of engineering applications in aerospace, automotive, and biomedical industries [1–4]. However, use of Mg alloys is often restricted by their limited ductility, formability, and fatigue strength [5]. These poor mechanical properties of Mg alloys are attributed to their hexagonal closed-packed (HCP) crystal structure, which exhibits a limited number of easy slip systems to accommodate deformation strain [6,7].

In order to improve the mechanical performance of Mg alloys, several manufacturing approaches have been proposed, including micro-alloying [8], equal-channel angular extrusion (ECAE) [9], and surface mechanical attrition treatment (SMAT) [10]. In addition to these processing approaches, a laser-based surface processing technology, laser shock peening (LSP), is exceptional due to its high process efficiency, flexibility, and controllability [11,12]. LSP is a surface processing process utilizing pulsed laser energy to introduce compressive residual stresses and a work-hardened layer to the surfaces of metallic materials for enhanced durability [13,14]. Recent studies indicate that LSP is promising to improve the engineering performance of Mg alloys

by enhancing their surface strength [15], biocompatibility [16], fatigue resistance [17], and anti-corrosion ability [18]. For instance, Ye et al. [15] showed that LSP resulted in the increase of surface hardness of AZ31B Mg alloy from 57 to 69 HV and the yield strength from 128 to 152 MPa. Vinodh [16] et al. reported that the corrosion rate of the Mg–calcium (Mg–Ca) alloy samples without laser processing was 2.5 times higher than that of the samples processed by LSP. In addition, laser processed samples exhibited a significantly improved biocompatibility. Ge et al. [19] investigated the effect of LSP on the stress corrosion cracking behavior of AZ31B Mg alloy and showed that the SCC susceptibility index of the LSP treated samples was decreased by 47.5% as compared to the as-received samples. Sealy et al. [20] studied the fatigue performance of Mg–Ca alloys subjected to LSP and found that the rotating bending fatigue life of the laser peened samples was ten times higher than that of the untreated samples.

Despite these experimental efforts on understanding the effect of LSP on enhancing performance of Mg alloys, little attention has been paid to study the surface microstructure evolution during LSP. Although surface grain refinement of Mg alloys during LSP was reported in [21,22], no particular investigation has been focused on elucidating the

* Corresponding author.

E-mail address: yliiao@unr.edu (Y. Liao).

formation of high density deformation twins as a result of surface plastic deformation with an ultrahigh strain rate of 10^6 – 10^7 /s in the LSP process. Deformation twinning in HCP structure plays a fundamental role in enhancing mechanical performance of Mg alloys [23,24]. In addition, the microstructural anisotropic response to LSP should be considered. A better understanding of twinning mechanisms in Mg alloys as subjected to LSP may lead to improved process development and control for optimized mechanical performance.

This research is to establish the process-microstructure relationship of Mg alloys as processed by LSP. A focus is placed on understanding deformation twinning mechanism. LSP experiments are conducted on a rolled AZ31B Mg alloy. The microstructures before and after laser processing are characterized using optical microscopy, electron backscatter diffraction (EBSD), and scanning electron microscope (SEM). The effect of laser intensity on the twin volume fraction is investigated. The surface hardness as associated with the twin density is measured. The mechanisms responsible for the formation of gradient twinning microstructures and the twinning-induced strain hardening effect are discussed. The anisotropic response to LSP in terms of grain orientation and the resultant microstructure and hardness improvement in Mg samples are compared and discussed.

2. Experiments

2.1. Materials

Rolled AZ31B Mg alloy block (3.0 wt% Al, 1.0 wt% Zn, Mg balance) purchased from MetalMart.com was used for experiments. Cubic samples with a dimension of 1 in. by 1 in. were machined from the block for LSP processing. Prior to laser processing, the samples were grinded using SiC sandpapers with different grit numbers (from 320 to 1200), followed by fine polishing using 3 μ m diamond suspension. Afterwards, the samples were ultrasonically cleaned in an ethanol solution.

2.2. LSP experiments

Fig. 1a shows a schematic view of the LSP configuration. In this work, a Q-switched Nd-YAG laser (Surelite III from Continuum, Inc.), operating at a wavelength of 1064 nm and a pulse width of 5 ns (full width at half maximum), was used to deliver the laser energy. The laser beam diameter was 2 mm. The laser power intensity was adjusted by adjusting the Q-switched delay time. Black tape with a thickness of 100 μ m was used as the ablative coating material. BK7 glass with a high shock impedance was used as the transparent confinement. LSP experiments were performed along the rolling direction (RD) of the specimen (Fig. 1b).

2.3. Microstructure characterization

The microstructure before and after LSP was characterized using Leica DM2700 optical microscope (OM), SM-7100FT field emission scanning electron microscope (FESEM), and electron backscattered microscope (EBSD). Samples for optical microscope characterization were prepared by sectioning, mounting, polishing, and etching with the acetic picral solution. (10 ml acetic acid + 4.2 g picric acid + 10 ml distilled water + 70 ml ethanol). EBSD characterization was performed in the stage control model with TSL data acquisition software on an area of 200 μ m by 200 μ m with a step size of 0.5 μ m. All the microstructure characterization was performed on a cross-section perpendicular to the ND.

2.4. Mechanical properties test

The surface micro-hardness of samples before and after laser processing were measured using a Wilson Hardness tester with a 500 g load and 10 s holding time. In order to study the effect of the gradient twinning microstructure on the material strength, in-depth hardness was measured from the top surface to a depth of 2300 μ m on TD-ND planes in Fig. 1b. An electrolytic polisher was used to remove the material layer by layer for in-depth hardness testing. At each depth, the hardness values were measured 5 times.

3. Results and discussion

3.1. Laser-induced shockwave pressure and propagation

In order to understand the process-microstructure relationship, first the shockwave pressure during LSP is theoretically estimated. According to the widely accepted Fabbro's laser shock processing mode (Eqs. (1)–(3) [13,25], the magnitude of shockwave pressure $P(t)$ can be estimated as a function of the shock impedance Z (confining media Z_1 and target material Z_2) and the laser intensity $I(t)$, where $L(t)$ is the layer thickness of laser-induced plasma, α is the efficiency of the interaction (≈ 0.1), and t is the time.

$$\frac{2}{Z} = \frac{1}{Z_1} + \frac{1}{Z_2} \quad (1)$$

$$\frac{dL(t)}{dt} = \frac{2}{Z} P(t) \quad (2)$$

$$I(t) = P(t) \frac{dL(t)}{dt} + \frac{3}{2\alpha} \frac{d}{dt} [P(t)L(t)] \quad (3)$$

In this work, $Z_1 = Z_{\text{glass}} = 1.44 \times 10^6 \text{ g/cm}^2\cdot\text{s}$, $Z_2 = Z_{\text{AZ31B}} = 1.01 \times 10^6 \text{ g/cm}^2\cdot\text{s}$ [26], and $I(t)$ is given by Eqs. (4) and (5) [27]:

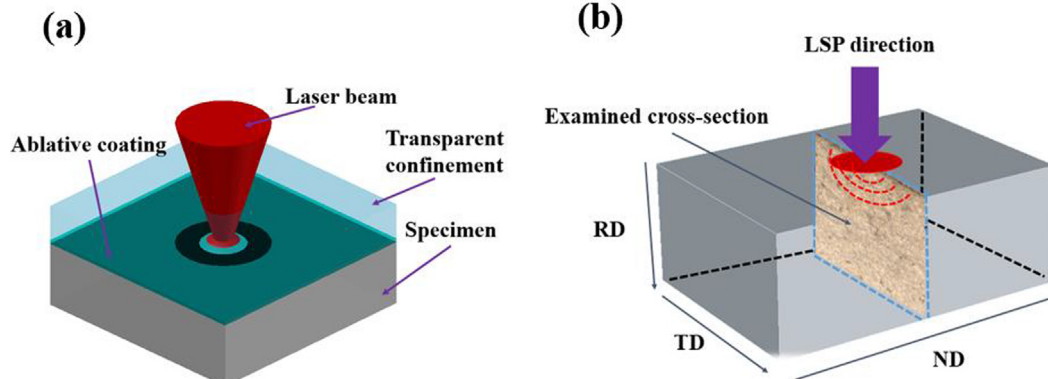


Fig. 1. Schematic illustrations of: (a) LSP experimental set up, and (b) LSP direction and examined cross-section of the processed specimen, where the RD, TD, and ND are rolling, transverse, and normal direction, respectively.

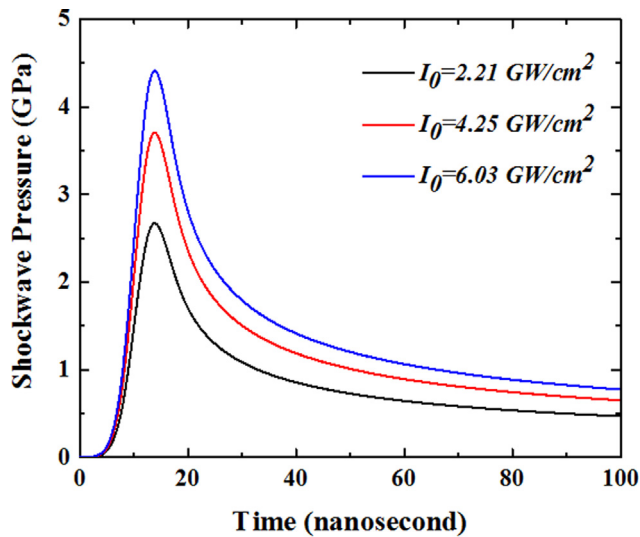


Fig. 2. The temporal evolution of laser shockwave pressure as affected by the laser intensity in LSP experiments, estimated by Fabbro's model.

$$I_0 = \frac{Q}{\pi(d/2)^2 \Delta t} \quad (4)$$

$$I(t) = I_0 \frac{1}{\sigma \sqrt{2\pi}} e^{-\frac{1}{2} \left(\frac{t-\mu}{\sigma} \right)^2} \quad (5)$$

where I_0 is the maximum laser intensity, Q is the pulse laser energy, d is the beam diameter, and Δt is the laser pulse duration. The value of σ and μ can be estimated from the effective laser duration FWHM (full width at half maximum), $FWHM = 2\sqrt{2 \ln 2} \sigma \approx 2.355\sigma = 5 \text{ ns}$ and $\mu = 6\sigma$.

Based on Eqs. (1)–(5), the temporal evolution of shockwave pressure for various laser intensities is calculated as shown in Fig. 2. It can be seen that the shockwave pressure in LSP experiments increases to their peak values within 20 ns and then decays gradually with time. As the shockwave propagates into the Mg block, the effective pressure decays with the increase of depth [28,29].

It is typically assumed that shock pressure follows a Gaussian spatial distribution, the spatially uniform shock pressure $P(t)$ relates to the spatially non-uniform shock pressure as [30]:

$$P(r, t) = P(t) \exp\left(-\frac{r^2}{2r_0^2}\right) \quad (6)$$

where r_0 is the laser beam radius, and r is the distance from the center of the laser beam.

3.2. Gradient twinning microstructure

Fig. 3 shows the initial microstructure of the specimen. It can be seen that the material has a twin-free equiaxed grain structure with an average grain size of $25 \mu\text{m}$ (Fig. 3a and c). The EBSD phase mapping indicates a strong basal texture where most basal planes align parallel to the rolling direction (Fig. 3b and d).

Optical microscopy images in Fig. 4 show the microstructure of the specimen processed by single pulse LSP with laser intensities of 2.21, 4.25, and 6.03 GW/cm^2 . It can be seen that a depth-dependent microstructure in the specimens is generated by LSP. In Fig. 4a, surface micro-indentations are observed on the top surfaces. A hemispherical distribution of twins can be identified and is marked by the red dashed lines in Fig. 4b, c, and d. With the increase of laser intensity, the depth of LSP affected zone increases. For instance, the depth of the twinned area is about $850 \mu\text{m}$ in the specimen processed by LSP with a laser intensity of 2.21 GW/cm^2 , while for the specimen processed by LSP

with a laser intensity of 6.03 GW/cm^2 , the twinned area reaches to around $1650 \mu\text{m}$. Moreover, a twin saturation or exhausted zone (i.e. the matrix is almost totally twinned) can be observed and marked by the blue dashed lines in Fig. 4c and d. The saturated and unsaturated twinning areas can be easily identified, since after etching with acetic picral solution, the twin exhausted area (Fig. 4e) exhibits a different color as compared to the unsaturated twin area (Fig. 4f).

EBSD analysis was conducted to characterize the gradient twinning microstructure generated by LSP. In Fig. 5, the three inverse pole figure (IPF) maps at different depths are picked from the examined cross-section of Mg alloy samples processed by LSP with a laser intensity of 6.03 GW/cm^2 . Compared with the initial microstructure, the texture and crystallographic orientation distribution are dramatically changed by LSP, owing to the growth of deformation twinning. At a depth of $500 \mu\text{m}$ within the twin saturated area, the parent grains are almost totally twinned. As the depth increases to $1000 \mu\text{m}$, twins in green and blue can be seen but the remaining parent grains can be identified. Some refined grains can be observed as well. At the depth of $1500 \mu\text{m}$, needle-like twins with a low density can be observed and the majority of the parent grains are not twinned.

Fig. 6 shows a detailed EBSD analysis of the microstructure of the sample processed by LSP with a laser intensity of 6.03 GW/cm^2 at a depth of $500 \mu\text{m}$. In Fig. 6a, both large and small grains can be observed. Very few parent grains can be seen, indicating twinning is saturated in this region. Fig. 6b and c show some local areas which contain small patches (in red) of remaining parent grains. The point to point misorientation line profiles show that the misorientations between the parent grain and twin bands are about 86° (Fig. 6d and e). This indicates that all the twin bands were generated by $\{10\bar{1}2\}$ twinning [24].

The effect of LSP on surface grain refinement of metallic materials has been extensively reported in literature [31,32]. Ge et al. [17] reported that nano-grains with an average size of 17.5 nm can be generated in the top surface of AZ31B Mg alloy through LSP, and the thickness of the nanostructured layer is around $20 \mu\text{m}$. Ren et al. [33] also demonstrated nano-structured surface layer can be fabricated in AZ91D Mg alloy by LSP. In Fig. 6a, some very small untwinned grains are observed, showing the grain refinement effect. However, the grain refinement in the samples subjected to LSP along the RD is not as conspicuous as in metals in which dislocations dominate the plastic deformation. In addition to the small grains, large grains can also be observed in Fig. 6a. Hong et al. [34] investigated the twin morphology and texture evolution of AZ31B Mg alloys subjected to compression along the TD. It was found that with a small deformation strain, the effective grain size tended to become smaller due to the grain refinement caused by twin nucleation. However, given a relatively large deformation strain, a grain coarsening effect was observed, leading to an increased grain size. The large grains observed in Fig. 6a could be attributed to the relatively large strain in the near-surface region. In contrast, no large grains are seen at the depth of $1500 \mu\text{m}$ (Fig. 7). The presence of large grains in Fig. 6a is abnormal in our AZ31B samples subjected to LSP because grain refinement after LSP is typical and significant in crystalline metals and alloys with FCC (face centered cubic) and BCC (body centered cubic) structures [31,35,36]. These abnormally large grains might be related to one of the dynamic recrystallization (DRX) mechanisms, i.e. discontinuous DRX by grain boundaries migration [37,38].

Most of previous investigations have attributed the surface nano-crystallization to high density dislocations generated by laser shock-wave. In our case, we also take into consideration the highly anisotropic mechanical behavior of Mg alloys. It is well known that for rolled Mg alloys, when the tensile stress is applied along the c-axis or the compression stress is applied perpendicular to the c-axis, as the case of LSP experiments in this paper, deformation twinning is the dominant mechanism responsible for the plastic deformation [39]. In fact, as the critical stress for $\{10\bar{1}2\}$ twinning is so small (comparable to basal slip

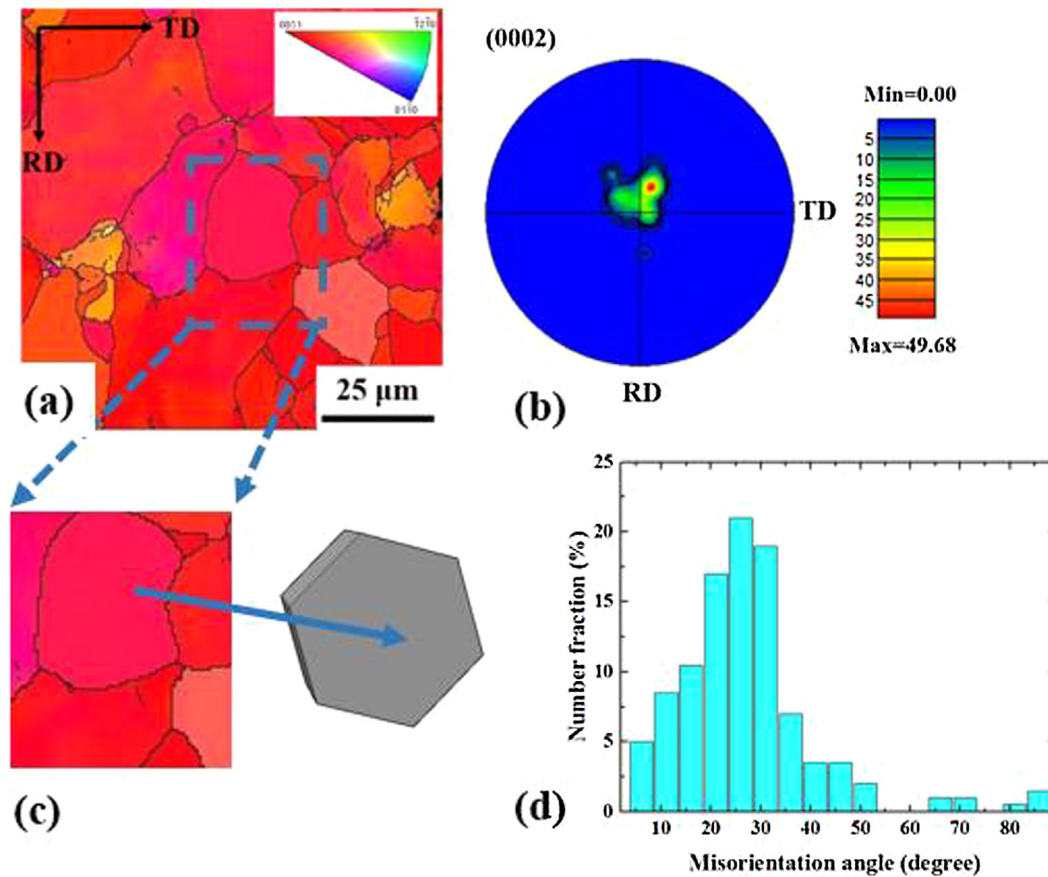


Fig. 3. Initial microstructure of the cross-section perpendicular to ND of the as-received rolled AZ31B Mg alloy. (a) Inverse pole figure map, (b) (0 0 0 2) pole figure, (c) a crystallographic orientation map, and (d) point to point misorientation angle distribution for grain boundaries.

and much lower than non-basal slip [40]), the plastic strain is mainly accommodated by deformation twinning rather than dislocation slip. Therefore, in the LSP process, if the laser shock loading is along the RD or TD direction, deformation twinning plays a dominant role in the microstructure-property relationship.

Fig. 7 shows the EBSD analysis of the microstructure of the specimen processed by LSP with a laser intensity of 6.03 GW/cm² at a depth of 1500 μm. It can be seen that the majority of the grains exhibit the initial basal texture, indicating a low twin density. Fig. 7a shows that the twins appear to be lenticular, which have a different

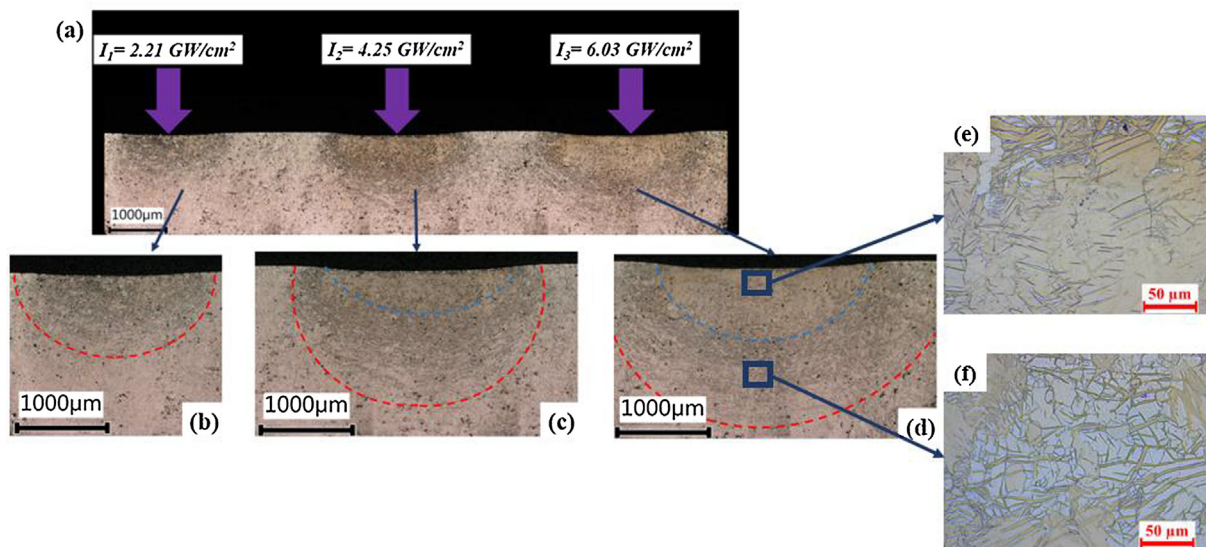


Fig. 4. Optical microscopy images showing microstructure of AZ31B Mg alloy processed by single pulse LSP: (a) An overview of the cross-section of laser processed samples with surface micro-indentations; (b), (c), and (d) microstructure of the specimens processed by LSP with a laser intensity of 2.21, 4.25, and 6.03 GW/cm², respectively; (e) twinning saturated area and (f) twinning unsaturated area.

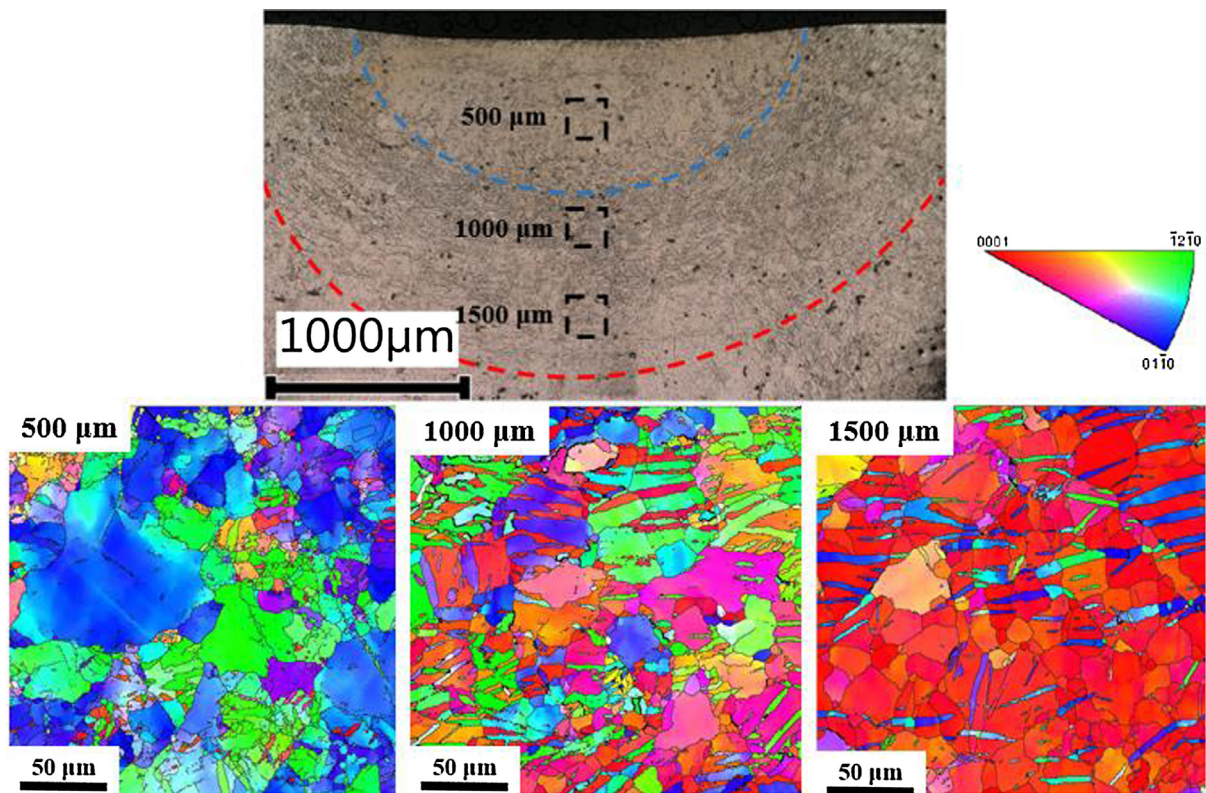


Fig. 5. EBSD analysis of the detailed microstructure in three different depths of the sample processed by LSP with a laser intensity of 6.03 GW/cm².

morphology as compared with the twins in Fig. 6a. Fig. 7b shows a local grain which contains four twin laths, and the misorientation profiles in Fig. 7c shows that those four twin laths have the same crystal orientation. Although {10 $\bar{1}$ 2} twinning has six possible twin variants, it can be seen that in most grains only one dominant twin variant is activated, as shown in Fig. 7b. However, some grains do have more than one variants, as denoted by “twin 2-1” and “twin 2-2” in Fig. 7c. The

activation of a twinning system strongly depends on the initial crystal texture and the direction shockwave pressure [41,42].

The evolution of the twin density and morphology with depth of the samples processed by LSP are presented in Fig. 8. Fig. 8a shows the effect of laser intensity on the gradient twinning microstructure of AZ31B Mg alloys generated by LSP. The value of d on each micrograph indicates the depth from the top surface where the microstructure is

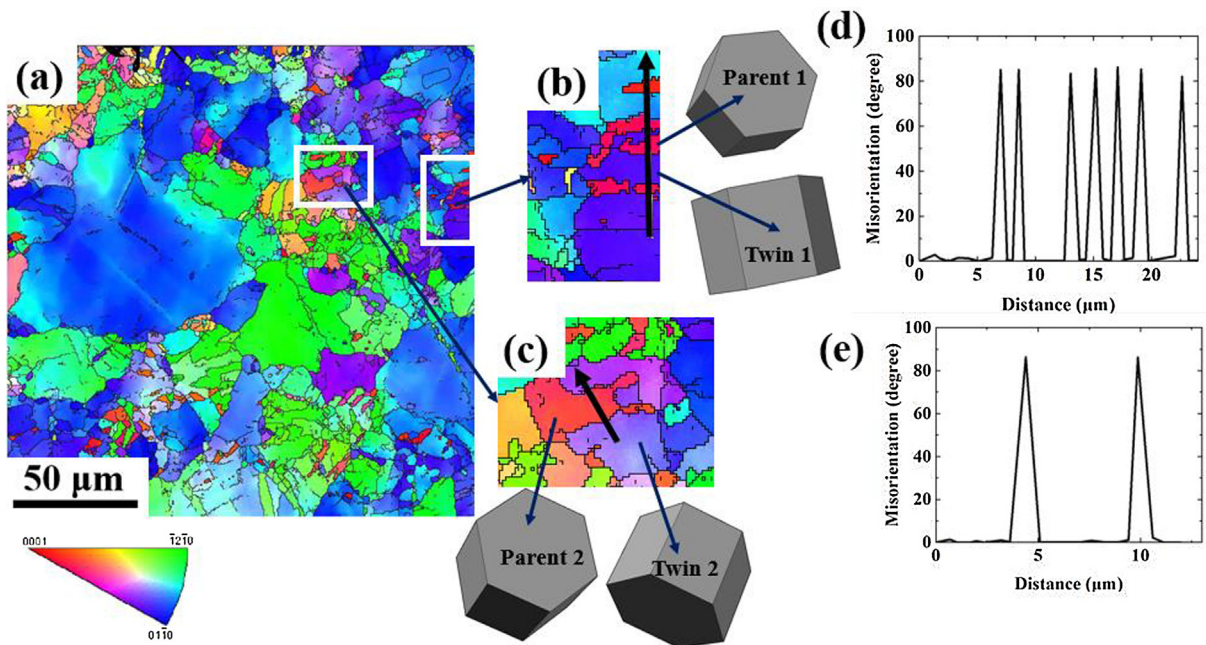


Fig. 6. Inverse pole figure maps and crystallographic orientation analysis of microstructure of sample processed by LSP with a laser intensity of 6.03 GW/cm² at a depth of 500 μm. (a) Inverse pole figure map; (b) and (c) crystallographic orientation maps obtained from (a); (d) and (e) point to point misorientation line profiles along the direction indicated as an arrow in (b) and (c), respectively.

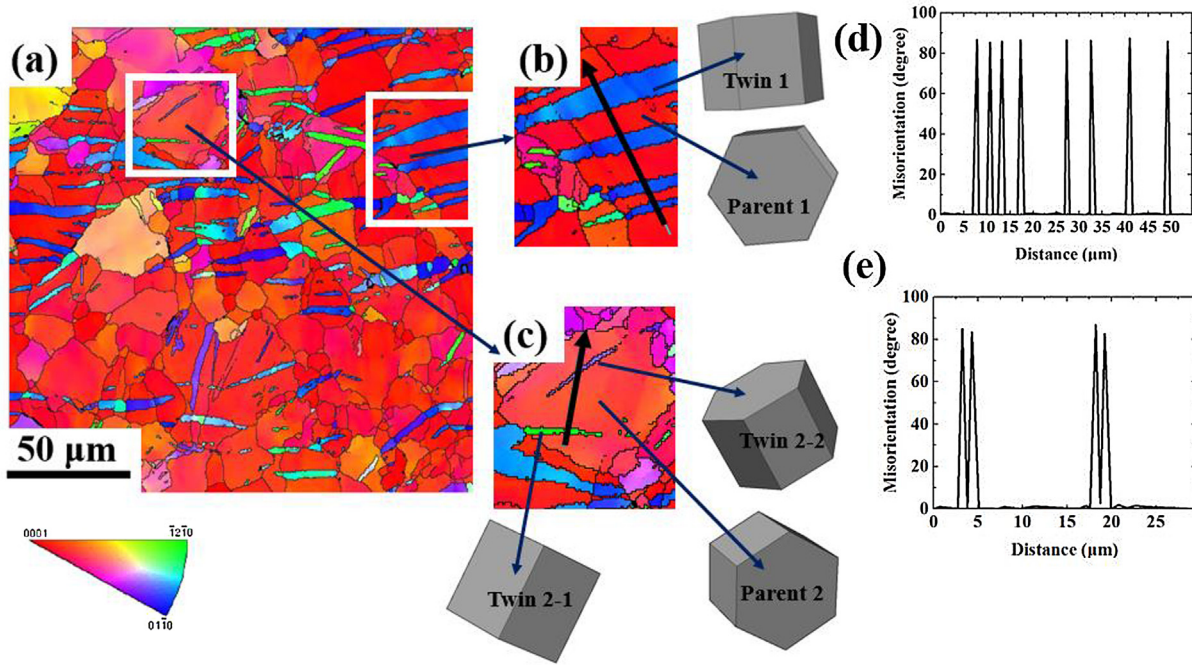


Fig. 7. Inverse pole figure maps and crystallographic orientation analysis of the microstructure of sample processed by LSP with a laser intensity of 6.03 GW/cm² at a depth of 1500 μm. (a) Inverse pole figure map; (b) and (c) crystallographic orientation maps obtained from (a); (d) and (e) point to point misorientation line profiles along the direction indicated as an arrow in (b) and (c), respectively.

characterized. Each micrograph has a dimension of 250 by 180 μm. The twin volume fraction (TVF) at each depth is summarized in Fig. 8b. The TVF is calculated using the methodology reported in [43] in which the volume fraction is counted as the fraction of the pixels occupied by the twins. The optical microscopy analysis (Fig. 8a) indicates a gradually decrease of twin density with increasing depth, which is consistent with the overall microstructure in Fig. 4. For example, at the depth of 90 μm, all the microstructures show a very high twin density, which are 82.3, 96.0, and 96.5% for the samples processed by LSP with a laser intensity of 2.21, 4.25, and 6.03 GW/cm², respectively. As the depth reaches 1530 μm, twins can barely be observed in the sample processed with a laser intensity of 2.21 GW/cm², and the twin densities for the samples processed with a laser intensity of 4.25 and 6.03 GW/cm² are 40.2% and 78.3%, respectively. Moreover, a higher laser intensity leads to a higher TVF at the same depth. For instance, at the depth of 1170 μm, the sample processed with a laser intensity of 6.03 GW/cm² shows a saturated twinning zone, while much fewer twins can be identified for the specimen processed with a laser intensity of 4.25 and 2.21 GW/cm². At the depth of 2250 μm, there is a small amount of twins (11.4%) for the sample processed with a laser intensity of 6.03 GW/cm², while no twins can be observed in the other two samples processed with a lower laser intensity.

In the LSP process, the amount of twin volume fraction in Mg alloys is related to the plastic strain that needs to be accommodated. Chen et al. [43] measured the contribution of extension twinning to plastic strain of AZ31B Mg alloy. The results show that when the tension load is along the *c*-axis or the compression load is perpendicular to the *c*-axis, the extension twinning dominates the plastic deformation. The quantitative expression for the contribution of deformation twinning to plastic strain can be given as [34,44].

$$\varepsilon_{\text{twin}} = f_{\text{twin}} \times \gamma_{\text{twin}} \times m \quad (7)$$

where $\varepsilon_{\text{twin}}$ denotes the macroscopic strain, f_{twin} is the twin volume fraction, γ_{twin} is the magnitude of twinning shear, and m is the average Schmid factor of the twinning systems. Eq. (7) explains the gradient twinning microstructure of Mg alloys generated by LSP. With an increase of depth, the laser shock pressure decays, and thus the value of

$\varepsilon_{\text{twin}}$ decreases, leading to the decrease of twin volume fraction. Moreover, since the shockwave peak pressure for laser intensities used in this study is much higher than the dynamic yield strength of the AZ31B Mg alloys (Fig. 2), a high plastic strain is expected at the near-surface area, resulting in the saturated twinning zone.

The deformation mechanism of the AZ31B Mg alloys processed by LSP along RD is illustrated in Fig. 9. Fig. 9a shows the initial crystal orientation for the as-received specimen, where the material exhibits the basal texture with the *a*-axis parallel to the RD. Fig. 9b shows the crystal reorientation by twinning when the material is subjected to laser shock loading along the *a*-axis direction. Note that although several different twin variants might be activated in one grain, the variant with the highest Schmid factor dominates, which agrees with the analysis by Hong et al. [34]. As shown in Fig. 9b, due to the laser shock loading, the initial crystals (marked by dark color) with the *c*-axis parallel to the ND are transferred to twin crystals (marked by green color) with *c*-axis perpendicular to the ND with a crystallographic lattice orientation of ~90°. This crystal reorientation is typical of {10 $\bar{1}$ 2} extension twinning [24].

3.3. Gradient strain hardening mechanism

To investigate the effect of gradient twinning microstructure on the mechanical properties of the AZ31B Mg alloy, micro-hardness tests at various depths were conducted as shown in Fig. 10. It can be noted that Vickers hardness numbers (VHN) of the specimen processed by LSP decrease with increasing depth till 60 VHN, which is the hardness of the base metal. The maximum VHNs for three different laser processing intensities are all around 74 VHN, indicating a saturation point for hardness improvement by LSP. The saturation of surface strength by LSP has also been reported for other metallic materials [14]. It is also observed in Fig. 10 that a higher laser intensity leads to a larger hardening depth. For example, by increasing laser intensity from 2.21 to 6.03 GW/cm², the depth of full-hardened layer (72 VHN) increases from around 500 to 1500 μm.

Surface hardening effect induced by LSP in metallic materials has been extensively studied. It is well accepted that the improved hardness

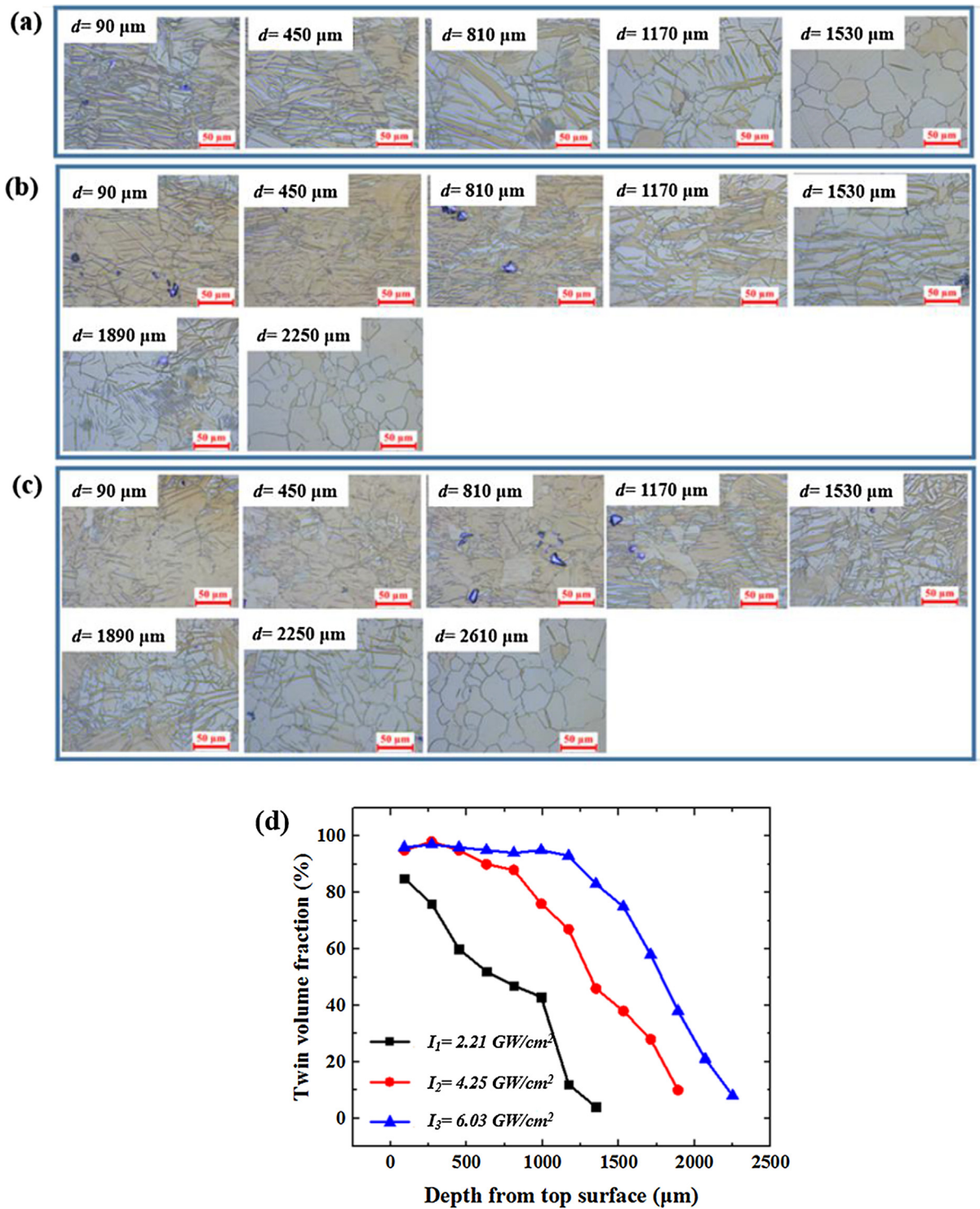


Fig. 8. Optical microscopy images of the in-depth microstructure of AZ31B Mg alloy samples processed by LSP with various laser intensities of (a) 2.21, (b) 4.25, and (c) 6.03 GW/cm². (d) Variation of twin volume fraction with depth in samples processed by LSP with different laser intensities.

is due to work hardening and grain refinement [31,32] for the metallic materials with a BCC or FCC crystal structure, such as steels and aluminum alloys [45,46] in which the plastic deformation is accommodated mainly by dislocation slip. However, for Mg alloys with a HCP crystal structure, in addition to grain refinement, deformation twinning is another important factor contributing to the surface hardening by LSP. Texture change by deformation twinning will change the deformation modes and thus affect the surface hardness. If an external compressive stress is applied along the a -axis, $\{10\bar{1}2\}$ twinning

dominated deformation will induce a relatively lower flow stress, whereas if a compressive stress is applied along the c -axis, the deformation mode is highly favorable for dislocation slip and contraction twinning, which have a higher CRSS (critical resolved shear stress), and thus induce a higher flow stress [34,42]. Knezevic et al. [47] proposed that the main contribution of extension twinning to the strain hardening in TD-RD compressed samples is texturing hardening. In this study, the crystal reorientation by LSP will change the deformation mode from an easy-to-deform direction (compression along a -axis) to a difficult-to-

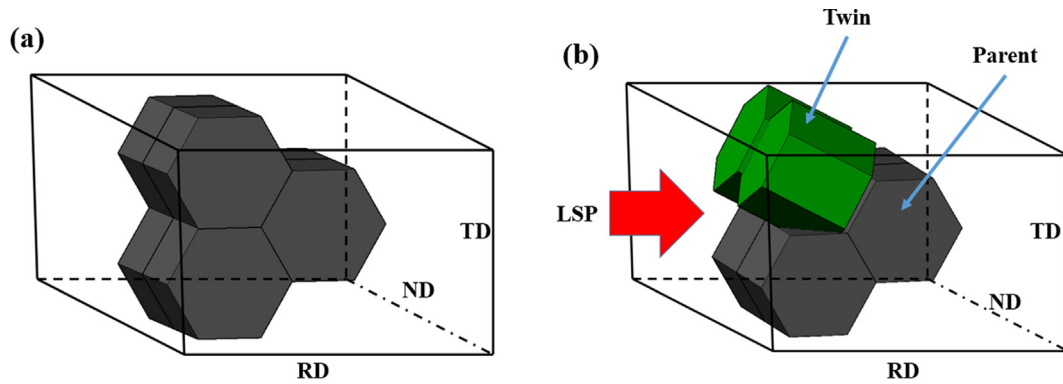


Fig. 9. Schematic of deformation mechanism of Mg alloys by LSP. (a) Initial crystal orientation, and (b) crystal reorientation by twinning after LSP.

deform direction (compression along *c*-axis). As a result, both grain refinement and texture change are expected to contribute to the surface hardening of Mg alloys processed by LSP.

3.4. Anisotropic microstructural and mechanical response to LSP

For textured Mg alloys, their anisotropic mechanical properties may lead to an anisotropic microstructural response to LSP. To study this effect, LSP experiments with a laser intensity of 2.21 GW/cm^2 were carried out both along ND and RD. As the SEM images shown in Fig. 11, high density twins can be observed when LSP is along the RD; in contrast, almost no twins can be observed when LSP is along the ND. This result is consistent with observation of the microstructure evolution under static compression along the ND conducted by previous researchers [48,49]. When a compressive stress is applied along the ND, the plastic deformation is mostly accommodated by dislocation slip on the basal and pyramidal planes [50]. Thus twinning microstructure cannot be achieved by LSP along ND. However, some refined grains can be identified in the near surface area in Fig. 11b, as marked by the yellow circle. Because the plastic deformation of Mg alloys is dominated by dislocation activities instead of twinning in compression along the ND [51,52], the grain refinement in the AZ31B processed by LSP along ND is attributed to the activation of high density dislocations, followed by recovery and recrystallization under the severe plastic strain at the ultrahigh strain rate of laser loading, similar to grain refinement in LSP processed steels [32], aluminum alloys [31], and titanium alloys [36].

The surface (RD-TD plane) hardness the AZ31B processed by LSP along the ND with different laser intensities were measured and the results were compared with those samples processed by LSP along the RD. As shown in Fig. 12, for the sample processed by LSP along ND with a laser intensity of 2.21 GW/cm^2 , the surface hardness increases from 63.2 VHN for the untreated specimen to 72.3 VHN, corresponding to a 14.4% increase. The increased surface hardness is mainly attributed to work hardening and grain refinement generated by LSP. As the laser

intensity increases from 2.21 GW/cm^2 to 6.03 GW/cm^2 , the surface hardness value only increases from 72.3 to 74.1 VHN, and this is due to the saturation of plastic deformation [11]. Moreover, it is noted that the surface hardness of the AZ31B before and after LSP along the ND are all slightly higher than those processed by LSP along the RD regardless of laser intensity. This difference is mainly attributed to the fact the strain hardening effect induced by dislocations is typically more prominent than it is induced by twinning [47]. Nevertheless, LSP along the ND and the RD can both effectively improve the surface hardness.

4. Conclusion

In this paper, a systematic study is carried out on the process-microstructure relationship of Mg alloys as processed by LSP. A focus is placed on understanding the deformation twinning mechanism and twinning-induced strain hardening effect during LSP. The twinning type, morphology, variation in TVF vs depth, and corresponding in-depth hardening effect are analyzed. Following conclusions can be drawn:

- (1) When LSP is along the RD, a gradient twinning microstructure is generated. The twins are identified as $\{10\bar{1}2\}$ extension twins. The density of twins decreases with increasing depth, and a higher laser intensity results in a deeper twinned zone.
- (2) A gradient hardness distribution well corresponds to the gradient twinning microstructure. The hardness of laser-processed samples decreases with an increase of depth from the saturation value of 74 VHN to the base value of 60 VHN. The LSP-induced strain hardening is attributed to the grain refinement and the texture change induced by nucleation and propagation of twinning structures.
- (3) Anisotropic microstructural and mechanical response to LSP is observed. High density twins can be observed when LSP is along the RD, whereas some refined grains can be observed when LSP is along the ND. LSP treatment of AZ31B Mg alloys along the ND and the RD

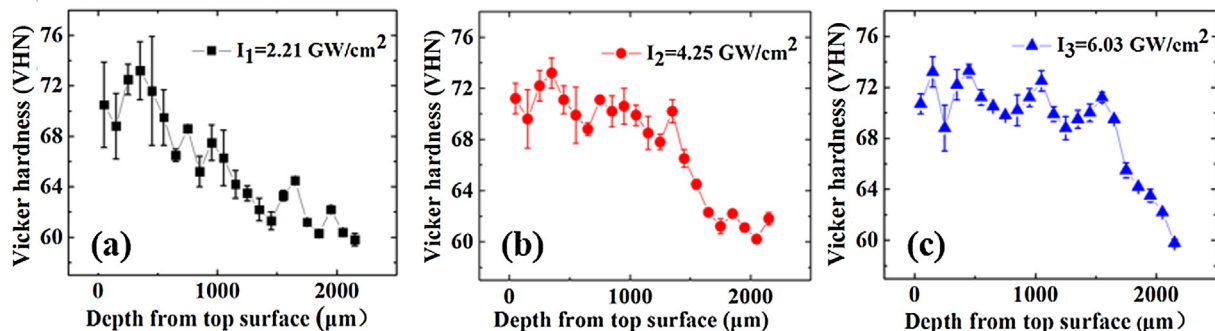


Fig. 10. In-depth hardness distribution of AZ31B Mg alloys processed by LSP with various laser intensities of: (a) 2.21, (b) 4.25, and (c) 6.03 GW/cm^2 .

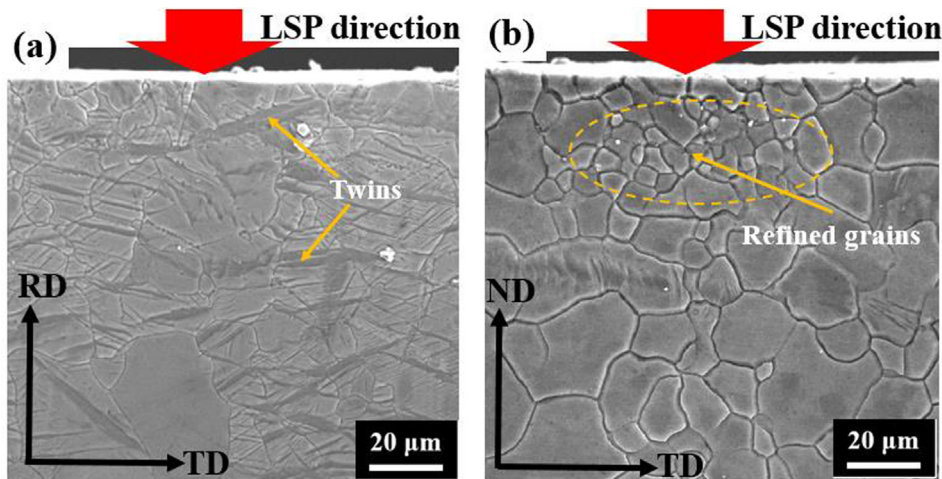


Fig. 11. SEM images of microstructure of the AZ31B Mg alloys processed by LSP along (a) RD, and (b) ND. Red arrow indicates the direction of laser shock loading.

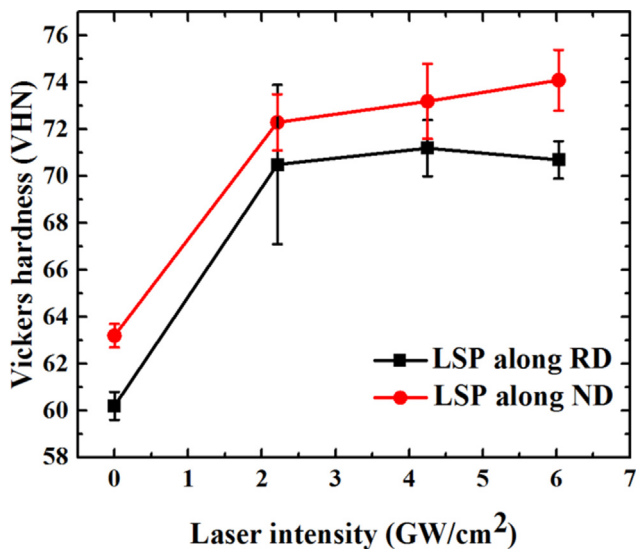


Fig. 12. Anisotropy in hardness improvement of the AZ31B Mg alloy processed by LSP with different laser intensities.

can both enhance the surface hardness.

Acknowledgements

The authors appreciate the financial support by startup funding from the Department of Mechanical Engineering at the University of Nevada, Reno. Y. Liao appreciates the support by ORAU Ralph E. Powe Junior Faculty Enhancement Award, 2016. B. Li thanks the support from US National Science Foundation (CMMI-1635088).

References

- [1] E. Aghion, B. Bronfin, Magnesium alloys development towards the 21st century, in: Mater. Sci. Forum, Trans Tech Publ, 2000, pp. 19–30.
- [2] M.P. Staiger, A.M. Pietak, J. Huadmai, G. Dias, Magnesium and its alloys as orthopedic biomaterials: a review, *Biomaterials* 27 (2006) 1728–1734.
- [3] M.K. Kulecki, Magnesium and its alloys applications in automotive industry, *Int. J. Adv. Manuf. Technol.* 39 (2008) 851–865.
- [4] X. Cao, M. Jahazi, J. Immarrigeon, W. Wallace, A review of laser welding techniques for magnesium alloys, *J. Mater. Process. Technol.* 171 (2006) 188–204.
- [5] S. Basu, E. Dogan, B. Kondori, I. Karaman, A. Benzerga, Towards designing anisotropy for ductility enhancement: a theory-driven investigation in Mg-alloys, *Acta Mater.* 131 (2017) 349–362.
- [6] S.R. Agnew, Ö. Duygulu, Plastic anisotropy and the role of non-basal slip in magnesium alloy AZ31B, *Int. J. Plasticity* 21 (2005) 1161–1193.
- [7] S.-B. Yi, C. Davies, H.-G. Brokmeier, R. Bolmaro, K. Kainer, J. Homeyer,

- Deformation and texture evolution in AZ31 magnesium alloy during uniaxial loading, *Acta Mater.* 54 (2006) 549–562.
- [8] N. Stanford, M. Barnett, The origin of “rare earth” texture development in extruded Mg-based alloys and its effect on tensile ductility, *Mater. Sci. Eng. A* 496 (2008) 399–408.
- [9] T. Mukai, M. Yamanai, H. Watanabe, K. Higashi, Ductility enhancement in AZ31 magnesium alloy by controlling its grain structure, *Scripta Mater.* 45 (2001) 89–94.
- [10] L. Chen, F. Yuan, P. Jiang, J. Xie, X. Wu, Mechanical properties and deformation mechanism of Mg-Al-Zn alloy with gradient microstructure in grain size and orientation, *Mater. Sci. Eng. A* 694 (2017) 98–109.
- [11] K. Ding, L. Ye, *Laser Shock Peening: Performance and Process Simulation*, Woodhead Publishing, 2006.
- [12] A. Telang, A. Gill, S. Mannava, V.K. Vasudevan, D. Qian, S.P. Teyseyre, Effects of Laser Shock Peening on SCC Behavior Of Alloy 600, in: Idaho National Laboratory (INL), 2013.
- [13] P. Peyre, R. Fabbro, Laser shock processing: a review of the physics and applications, *Opt. Quantum Electron.* 27 (1995) 1213–1229.
- [14] C.S. Montross, T. Wei, L. Ye, G. Clark, Y.-W. Mai, Laser shock processing and its effects on microstructure and properties of metal alloys: a review, *Int. J. Fatigue* 24 (2002) 1021–1036.
- [15] X.N. Hou, H.F. Qin, H.Y. Gao, S. Mankoci, R.X. Zhang, X.F. Zhou, Z.C. Ren, G.L. Doll, A. Martini, N. Sahai, Y.L. Dong, C. Ye, A systematic study of mechanical properties, corrosion behavior and biocompatibility of AZ31B Mg alloy after ultrasonic nanocrystal surface modification, *Mater. Sci. Eng. C-Mater.* 78 (2017) 1061–1071.
- [16] V.K. Caralapatti, S. Narayanswamy, Effect of high repetition laser shock peening on biocompatibility and corrosion resistance of magnesium, *Opt. Laser Technol.* 88 (2017) 75–84.
- [17] M.-Z. Ge, J.-Y. Xiang, Effect of laser shock peening on microstructure and fatigue crack growth rate of AZ31B magnesium alloy, *J. Alloy. Compd.* 680 (2016) 544–552.
- [18] X. Li, Y. Zhang, J. Chen, Y. Lu, Effect of laser shock processing on stress corrosion cracking behavior of AZ31 magnesium alloy at slow strain rate, *Mater. Sci. Technol.* 29 (2013) 626–630.
- [19] M.-Z. Ge, J.-Y. Xiang, L. Yang, J. Wang, Effect of laser shock peening on the stress corrosion cracking of AZ31B magnesium alloy in a simulated body fluid, *Surf. Coat. Technol.* 310 (2017) 157–165.
- [20] M. Sealy, Y. Guo, R. Caslaru, J. Sharkins, D. Feldman, Fatigue performance of biodegradable magnesium–calcium alloy processed by laser shock peening for orthopedic implants, *Int. J. Fatigue* 82 (2016) 428–436.
- [21] M.-Z. Ge, J.-Y. Xiang, Z. Fan, Y. Lu, W. Lei, Effect of laser energy on microstructure of Mg-3Al-1Zn alloy treated by LSP, *J. Alloy. Compd.* 734 (2018) 266–274.
- [22] K. Luo, B. Liu, L. Wu, Z. Yan, J. Lu, Tensile properties, residual stress distribution and grain arrangement as a function of sheet thickness of Mg–Al–Mn alloy subjected to two-sided and simultaneous LSP impacts, *Appl. Surf. Sci.* 369 (2016) 366–376.
- [23] F. Zhang, M. Hao, F. Wang, C. Tan, X. Yu, H. Ma, H. Cai, Role of 10–12 twinning and detwinning in the shock-hardening behavior of rolled Mg–3Al–1Zn alloy, *Scripta Mater.* 67 (2012) 951–954.
- [24] J.W. Christian, S. Mahajan, Deformation twinning, *Prog. Mater. Sci.* 39 (1995) 1–157.
- [25] R. Fabbro, J. Fournier, P. Ballard, D. Devaux, J. Virmont, Physical study of laser-produced plasma in confined geometry, *J. Appl. Phys.* 68 (1990) 775–784.
- [26] S.P. Marsh, *LASL Shock Hugoniot Data*, Univ of California Press, 1980.
- [27] Y. Cao, Ablation and plasma effects during nanosecond laser matter interaction in air and water, in: Purdue University, 2015.
- [28] J. Lloyd, J. Clayton, R. Becker, D. McDowell, Simulation of shock wave propagation in single crystal and polycrystalline aluminum, *Int. J. Plast.* 60 (2014) 118–144.
- [29] Z. Zhang, G. Gogos, Theory of shock wave propagation during laser ablation, *Phys. Rev. B* 69 (2004) 235403.
- [30] W. Zhang, Y.L. Yao, Micro scale laser shock processing of metallic components,

- Trans.-Am. Soc. Mech. Eng. J. Manuf. Sci. Eng. 124 (2002) 369–378.
- [31] J. Lu, K. Luo, Y. Zhang, C. Cui, G. Sun, J. Zhou, L. Zhang, J. You, K. Chen, J. Zhong, Grain refinement of LY2 aluminum alloy induced by ultra-high plastic strain during multiple laser shock processing impacts, *Acta Mater.* 58 (2010) 3984–3994.
- [32] J. Lu, K. Luo, Y. Zhang, G. Sun, Y. Gu, J. Zhou, X. Ren, X. Zhang, L. Zhang, K. Chen, Grain refinement mechanism of multiple laser shock processing impacts on ANSI 304 stainless steel, *Acta Mater.* 58 (2010) 5354–5362.
- [33] X. Ren, X. Yang, W. Zhou, J. Huang, Y. Ren, C. Wang, Y. Ye, L. Li, Thermal stability of surface nano-crystallization layer in AZ91D magnesium alloy induced by laser shock peening, *Surf. Coat. Technol.* (2017).
- [34] S.-G. Hong, S.H. Park, C.S. Lee, Role of 10–12 twinning characteristics in the deformation behavior of a polycrystalline magnesium alloy, *Acta Mater.* 58 (2010) 5873–5885.
- [35] X. Nie, W. He, L. Zhou, Q. Li, X. Wang, Experiment investigation of laser shock peening on TC6 titanium alloy to improve high cycle fatigue performance, *Mater. Sci. Eng. A* 594 (2014) 161–167.
- [36] L. Zhou, Y. Li, W. He, G. He, X. Nie, D. Chen, Z. Lai, Z. An, Deforming TC6 titanium alloys at ultrahigh strain rates during multiple laser shock peening, *Mater. Sci. Eng. A* 578 (2013) 181–186.
- [37] R. Doherty, D. Hughes, F. Humphreys, J. Jonas, D.J. Jensen, M. Kassner, W. King, T. McNelley, H. McQueen, A. Rollett, Current issues in recrystallization: a review, *Mater. Sci. Eng. A* 238 (1997) 219–274.
- [38] S. Fatemi-Varzaneh, A. Zarei-Hanzaki, H. Beladi, Dynamic recrystallization in AZ31 magnesium alloy, *Mater. Sci. Eng. A* 456 (2007) 52–57.
- [39] N.-T. Nguyen, O.S. Seo, C.A. Lee, M.-G. Lee, J.-H. Kim, H.Y. Kim, Mechanical behavior of AZ31B Mg alloy sheets under monotonic and cyclic loadings at room and moderately elevated temperatures, *Materials* 7 (2014) 1271–1295.
- [40] K. Máthi, G. Csizsár, J. Čapek, J. Gubicza, B. Clausen, P. Lukáš, A. Vinogradov, S. Agnew, Effect of the loading mode on the evolution of the deformation mechanisms in randomly textured magnesium polycrystals—comparison of experimental and modeling results, *Int. J. Plast.* 72 (2015) 127–150.
- [41] C. Tomé, R.A. Lebensohn, U. Kocks, A model for texture development dominated by deformation twinning: application to zirconium alloys, *Acta Metall. Mater.* 39 (1991) 2667–2680.
- [42] H. Fan, S. Aubry, A. Arsenlis, J.A. El-Awady, The role of twinning deformation on the hardening response of polycrystalline magnesium from discrete dislocation dynamics simulations, *Acta Mater.* 92 (2015) 126–139.
- [43] P. Chen, B. Li, D. Culbertson, Y. Jiang, Contribution of extension twinning to plastic strain at low stress stage deformation of a Mg-3Al-1Zn alloy, *Mater. Sci. Eng. A* 709 (2018) 40–45.
- [44] A. Ghaderi, M.R. Barnett, Sensitivity of deformation twinning to grain size in titanium and magnesium, *Acta Mater.* 59 (2011) 7824–7839.
- [45] Y. Liao, S. Suslov, C. Ye, G.J. Cheng, The mechanisms of thermal engineered laser shock peening for enhanced fatigue performance, *Acta Mater.* 60 (2012) 4997–5009.
- [46] B. Mao, A. Siddaiah, P.L. Menezes, Y. Liao, Surface texturing by indirect laser shock surface patterning for manipulated friction coefficient, *J. Mater. Process. Technol.* 257 (2018) 227–233.
- [47] M. Knezevic, A. Levinson, R. Harris, R.K. Mishra, R.D. Doherty, S.R. Kalidindi, Deformation twinning in AZ31: influence on strain hardening and texture evolution, *Acta Mater.* 58 (2010) 6230–6242.
- [48] X. Guo, A. Chapuis, P. Wu, S. Agnew, On twinning and anisotropy in rolled Mg alloy AZ31 under uniaxial compression, *Int. J. Solids Struct.* 64 (2015) 42–50.
- [49] N. Dudamel, I. Ulacia, F. Gálvez, S. Yi, J. Bohlen, D. Letzig, I. Hurtado, M.T. Pérez-Prado, Twinning and grain subdivision during dynamic deformation of a Mg AZ31 sheet alloy at room temperature, *Acta Mater.* 59 (2011) 6949–6962.
- [50] M.T. Tucker, M.F. Horstemeyer, P.M. Gullett, H. El Kadiri, W.R. Whittington, Anisotropic effects on the strain rate dependence of a wrought magnesium alloy, *Scripta Mater.* 60 (2009) 182–185.
- [51] N. Stanford, K. Sotoudeh, P. Bate, Deformation mechanisms and plastic anisotropy in magnesium alloy AZ31, *Acta Mater.* 59 (2011) 4866–4874.
- [52] S. Yi, J. Bohlen, F. Heinemann, D. Letzig, Mechanical anisotropy and deep drawing behavior of AZ31 and ZE10 magnesium alloy sheets, *Acta Mater.* 58 (2010) 592–605.